Sustainable Energy & Fuels

ROYAL SOCIETY OF CHEMISTRY

PAPER

View Article Online
View Journal | View Issue

Check for updates

Cite this: *Sustainable Energy Fuels*, 2021, **5**, 4710

A cobalt oxide–polypyrrole nanocomposite as an efficient and stable electrode material for electrocatalytic water oxidation†

Daniela V. Morales,‡[ab] Catalina N. Astudillo,‡[a] Veronica Anastasoaie,‡[ac] Baptiste Dautreppe,[a] Bruno F. Urbano,[d] Bernabé L. Rivas,[d] Chantal Gondran,[a] Dmitry Aldakov,[e] Benoit Chovelon,[fg] Dominique André,[f] Jean-Luc Putaux,[h] Christine Lancelon-Pin,[h] Selim Sirach,[a] Eleonora-Mihaela Ungureanu,[c] Cyrille Costentin,[ai] Marie-Noëlle Collomb *[a] and Jérôme Fortage *[a]

Developing electrolyzers operating under neutral or near-neutral conditions with catalysts based only on earth-abundant metals is highly desirable with a view to reduce the cost of hydrogen production from the water splitting reaction and avoid the environmental issues related to corrosion usually encountered with alkaline electrolyzers. Herein, we report a highly active and stable anode material for the oxygen evolution reaction (OER) under mild-pH conditions based on cobalt oxide-nanoparticles embedded into a poly(pyrrole-alkylammonium) matrix (denoted as PPN^+-CoO_x). Examples of hybrid materials combining metal oxide nanoparticles as OER catalysts within a polymer film are still rare. However, they are very promising to control the formation and the size of metal particles in view of enhancing the electrochemically active surface area and thus the electrocatalytic performances. Our strategy consists in electroprecipitating Co^0 nanoparticles by the reduction of an anionic cobalt oxalate complex into a cationic PPN^+ film, the latter being previously deposited onto an electrode surface by electropolymerization. The Co^0 nanoparticles within the composite are then partially *in situ* oxidized under air exposure to CoO, and then finally fully oxidized to CoO_x by successive scans between 0 and 1.2 V *vs.* Ag/AgCl in a borate buffer at pH 9.2. This nanocomposite material is highly structured with around 30 nm-large CoO_x nanoparticles well dispersed into the polypyrrole film conferring a high OER electrocatalytic activity at a near neutral pH of 9.2 with exceptional values of mass activity and turnover frequency of 3.01 A mg^{-1} and 0.46 s^{-1} respectively, at an overpotential of 0.61 V and with a cobalt loading of 1.34 μg cm^{-2}. These performances place the PPN^+-CoO_x electrode among the most active anodes described in the literature employing cobalt oxide under mild pH conditions. In addition, when the PPN^+-CoO_x material is electrodeposited on carbon paper with a higher roughness than a simple carbon electrode, the physisorption of the film on the electrode is considerably enhanced resulting in a stable catalytic current for over more than 43 h. Post electrolysis characterization by SEM and EDX confirms the integrity of the PPN^+-CoO_x material after many hours of electrocatalysis. This demonstrates the beneficial role of the polypyrrole matrix in the achievement of very stable and highly active anodes for water oxidation.

Received 11th March 2021
Accepted 5th August 2021

DOI: 10.1039/d1se00363a

rsc.li/sustainable-energy

Open Access Article. Published on 05 August 2021. Downloaded on 9/22/2024 5:52:21 AM.
This article is licensed under a Creative Commons Attribution-NonCommercial 3.0 Unported Licence.

1. Introduction

Molecular hydrogen (H_2) is considered as the cleanest energy carrier of the future and one of the best alternatives to fossil fuels. Indeed, H_2 can be used in a fuel cell in the presence of oxygen to produce electricity with a relatively good conversion efficiency of around 50%, while releasing only water as the by-product.[1,2] However, most of the worldwide H_2 is currently industrially produced from fossil fuels *via* the steam reforming

[a]*Univ. Grenoble Alpes, CNRS, DCM, 38000 Grenoble, France. E-mail: jerome.fortage@univ-grenoble-alpes.fr; marie-noëlle.collomb@univ-grenoble-alpes.fr*
[b]*Department of Environmental Chemistry, Faculty of Sciences, Universidad Católica de La Santísima Concepción, Concepción, Chile*
[c]*Department of Inorganic Chemistry, Physical Chemistry and Electrochemistry, Faculty of Applied Chemistry and Materials Science, University Politehnica of Bucharest, Splaiul Independentei, 313, 060042 Bucharest, Romania*
[d]*Polymer Department, Faculty of Chemistry, University of Concepción, Concepción, Chile*
[e]*Univ. Grenoble Alpes, CNRS, CEA, IRIG, SyMMES, 38000 Grenoble, France*
[f]*Unit Nutritional and Hormonal Biochemistry-Institut de Biologie et de Pathologie, CHU De Grenoble Site Nord, F-38041, Grenoble, France*
[g]*Univ. Grenoble Alpes, DPM UMR 5063, F-38041 Grenoble, France*
[h]*Univ. Grenoble Alpes, CNRS, CERMAV, F-38000 Grenoble, France*
[i]*Université de Paris, 75013 Paris, France*

† Electronic supplementary information (ESI) available: See DOI: 10.1039/d1se00363a

‡ D. V. M., C. N. A. and V. A. contributed equally to this work.

This journal is © The Royal Society of Chemistry 2021

Open Access Article. Published on 05 August 2021. Downloaded on 9/22/2024 5:52:21 AM.
This article is licensed under a Creative Commons Attribution-NonCommercial 3.0 Unported Licence.

process, releasing CO_2, a greenhouse gas.[3] Another process, namely water electrolysis, is very attractive since it can produce hydrogen from water without using fossil raw materials, and could compete with steam reforming provided that clean, renewable and low-cost electricity is employed.[4,5] Basically, an electrolyzer consists of an anode and a cathode, respectively, for water oxidation to oxygen (*i.e.* oxygen evolution reaction, denoted as OER) and water reduction to hydrogen (*i.e.* hydrogen evolution reaction, denoted as HER), associated with a polymeric solid-state electrolyte, which is usually a proton exchange membrane (PEM) like Nafion®, or with a liquid alkaline electrolyte (*i.e.* a 20–40 wt% aqueous KOH solution).[6,7] PEM electrolyzers usually employ metallic Pt and IrO_2 electrocatalysts at the cathode and anode, respectively, and operate under strongly acidic conditions between 50 and 80 °C with high current densities up to 2 A cm^{-2}.[7,8] However, the high cost of rare metal-based electrocatalysts and the perfluorinated Nafion®-based membrane makes PEM electrolysis an expensive technology and thus questionable for mass production of H_2. By contrast, alkaline electrolysis is a much cheaper technology since it requires only nickel, an earth-abundant metal as the electrocatalyst, deposited on stainless steel electrodes for the cathode and anode, both being separated by a simple diaphragm conductive for hydroxide ions.[7,9] Nevertheless, such alkaline electrolyzers exhibit lower current densities (from 0.2 to 0.4 A cm^{-2} at 80 °C) compared to PEM electrolyzers and suffer from corrosion, which necessitates extensive maintenance and causes environmental and safety issues for operating personnel.[10] In order to avoid the problems related to corrosion and reduce the global cost of hydrogen produced from the electrocatalytic water-splitting reaction, it is of utmost importance to develop electrolyzers that efficiently work under neutral or near-neutral conditions with a cheap membrane along with electrocatalysts based on earth-abundant metals.[11]

The OER occurring at the anode is the bottleneck of the water splitting reaction and is more challenging than the HER at the cathode, more specifically at neutral or near-neutral pH, due to its sluggish kinetics and large anodic overpotential.[12–15] Several earth-abundant metal oxides such as Fe, Mn, Cu, Co and Ni and their alloys have been investigated as electrocatalysts for the OER under mild pH conditions.[11] Among them, cobalt oxide (CoO_x) has been intensively studied by many groups under alkaline conditions.[16–45] Originally identified as an electrocatalyst for water oxidation at pH 14 in 1950 by El Wakkad and Hickling,[46] CoO_x received renewed interest in 2008, owing to the work of Nocera and co-workers demonstrating that thin films of this earth-abundant metal oxide electrodeposited on an electrode surface in a proton-accepting phosphate (pH 7)[23,24] or borate (pH 9.2)[24] buffer are also very active OER electrocatalysts under such neutral or near-neutral conditions. A key factor for the performance of an electrocatalyst is its nanostructuration, the efficiency being significantly improved by increasing the active area/volume ratio, while reducing the cost of manufacture. However, the reduction of the particle size to increase the specific surface area of the catalyst leads to a reduction in their stability and can lead to aggregation. To overcome such limitations, we recently reported an original electrochemical approach to design nanocomposite electrode materials in which iridium or nickel oxide nanoparticles of small sizes (2–21 nm) are electrogenerated in a polypyrrole-alkylammonium matrix (denoted as PPN^+) of controllable thickness, previously deposited on the electrode surface by electropolymerization of the pyrrole monomer (3-pyrrole-1-yl-propyl)-triethylammonium (denoted as PN^+) (Scheme 1 and S1†).[47,48] These anodes displaying high OER activity prove to be much more effective and stable for electrocatalytic water oxidation than thin films of MO_x anodes (M = Ir or Ni) directly deposited on the electrode surface. Although examples of nanocomposites combining metal oxide particles and a polymer film for electrocatalytic water oxidation are quite rare,[47–50] these results highlight that such hybrid materials are very promising to control the formation and the size of metal particles and thus positively influence the catalytic behaviour and the stability of the anode.[51]

In this context, we have extended this interesting strategy of designing an efficient nanocomposite material to cobalt oxide and we report herein a very active and stable anode for the OER operating at pH 9.2 based on a cobalt oxide–poly(pyrrole-alkylammonium) nanocomposite (denoted as PPN^+-CoO_x). The PPN^+-CoO_x nanocomposite material electrodeposited onto vitreous carbon (denoted as C) or indium tin oxide (ITO) electrodes has been characterized by various electrochemical and microscopy techniques and the amount of cobalt was also quantified by inductively coupled plasma mass spectrometry (ICP-MS). The electrocatalytic properties of this nanocomposite material towards water oxidation have been evaluated in a borate buffer at pH 9.2 and compared with those of CoO_x-based anodes of the literature under similar catalytic conditions and with those of CoO_x films directly deposited on a naked electrode by the same electrochemical procedure. The objective was to highlight the beneficial role of the PPN^+ matrix in generating non-agglomerated CoO_x particles with higher OER activity.

2. Results and discussion

2.1. Electrosynthesis and electrochemical characterization of cobalt oxide and poly(pyrrole-alkylammonium)–cobalt oxide nanocomposite electrode materials

The four-step electrochemical procedure used to prepare the C or ITO/PPN^+-CoO_x modified electrodes is depicted in Scheme 1. For analytical electrochemical studies, C electrodes (surface of 0.071 cm^2) were used for film deposition, while larger surface ITO electrodes (surface of 1.0 cm^2) were employed for microscopy studies (see below). The first step consists of the electropolymerization in acetonitrile of PN^+ (4 mM) at the electrode surface at an applied potential of +0.95 V *vs.* $Ag/AgNO_3$ for an anodic charge of 4 mC.[48] The surface coverage in ammonium units Γ_{N^+} (mol cm^{-2}) corresponding to the amount of polypyrrole deposited on the electrode was estimated to be 1.20 ($\pm$0.1) $\times$ 10^{-7} mol cm^{-2} by the integration of the reversible redox process of polypyrrole (see the ESI†). In a second step, the PPN^+ electrode is dipped for one hour in an aqueous borate buffer at pH 6 (0.1 M Na_2SO_4 and 0.1 M H_3BO_3) containing

Open Access Article. Published on 05 August 2021. Downloaded on 9/22/2024 5:52:21 AM.
This article is licensed under a Creative Commons Attribution-NonCommercial 3.0 Unported Licence.

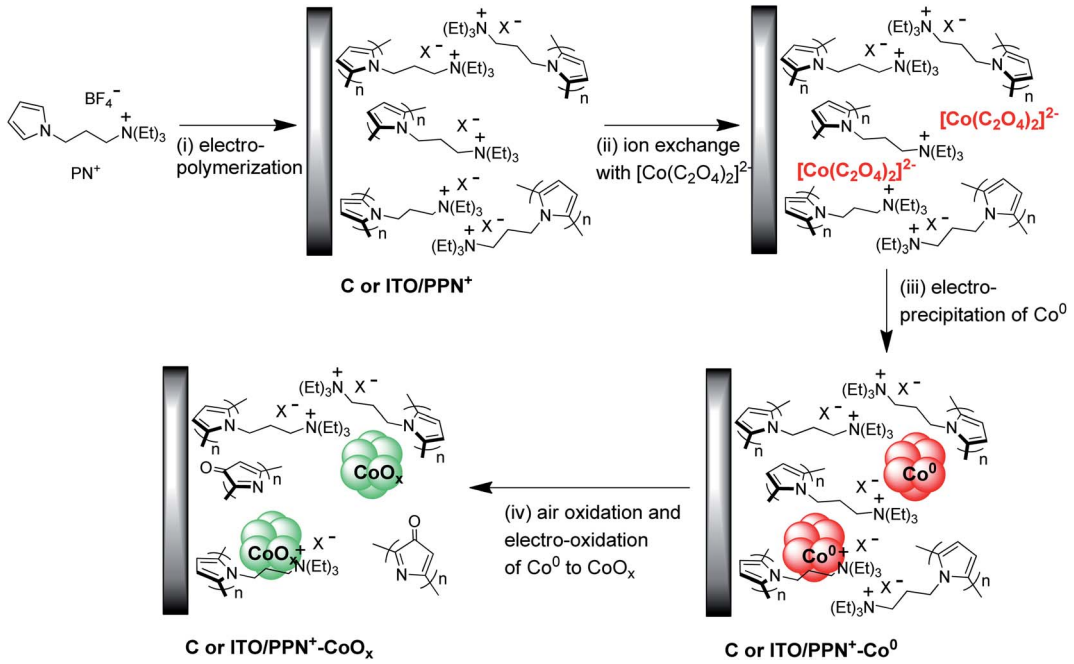

Scheme 1 General strategy for the electrosynthesis of poly(pyrrole-alkylammonium)/CoO_x nanocomposite film modified electrodes. (i) Formation of PPN^+ by oxidative electropolymerization of monomer PN^+ (4 mM) at E_{app} = +0.95 and +1.1 V *vs.* Ag/$AgNO_3$ in CH_3CN, 0.1 M $[Bu_4N]ClO_4$, respectively, for C and ITO electrodes; (ii) incorporation of $[Co(C_2O_4)_2]^{2-}$ into PPN^+ upon soaking for 1 h in a 0.1 M borate buffer solution (pH 6) of 4 mM $CoSO_4$, 20 mM $Na_2C_2O_4$ and 0.1 M Na_2SO_4; (iii) electroprecipitation of Co^0 within PPN^+ at E_{app} = −1.3 and −1.5 V *vs.* Ag/AgCl, respectively, for C and ITO electrodes, in the 0.1 M borate buffer solution (pH 6) of cobalt oxalate; (iv) air oxidation and electro-oxidation of Co^0 to CoO_x *via* 5 consecutive cycles between 0 and +1.2 V *vs.* Ag/AgCl in a 0.1 M borate buffer solution (pH 9.2).

$CoSO_4$ (4 mM) and $Na_2C_2O_4$ (20 mM), to incorporate by ion exchange within the cationic polypyrrole film[47,48,52–54] an anionic cobalt oxalate complex, most probably in the form of $[Co(C_2O_4)_2]^{2-}$ generated *in situ*. The Co^0 nanoparticles were then electrogenerated within the film by the reduction of the cobalt oxalate complex inserted into the polymer at an applied potential of −1.3 V *vs.* Ag/AgCl for a cathodic charge of 4 mC (Fig. S1†). Of note, in this article, the potentials are given *versus* Ag/AgCl for all electrochemical experiments performed in aqueous solution. During this electroreduction step, the C/PPN^+ modified electrode is maintained in the cobalt oxalate solution (0.1 M borate buffer at pH 6). For comparison purposes, Co^0 particles were also electrodeposited on naked C electrodes (without PPN^+) from the same cobalt oxalate aqueous solution using also a cathodic charge of 4 mC. Typically for Co^0 electrodeposition on C and in C/PPN^+ electrodes, about 130–170 s are required to pass a cathodic charge of 4 mC (Fig. S1†). A cathodic potential of −1.3 V for Co^0 electrogeneration on naked C and C/PPN^+ electrodes was chosen from the cyclic voltammetry (CV) of the cobalt oxalate solution recorded in borate buffer at pH 6 (Fig. 1).

In the CV shown in Fig. 1, a large irreversible process corresponding to the reduction of Co^{2+} (coordinated to oxalate) to metallic Co^0 leading to its deposition at the electrode surface starts at −1.0 V. The Co^{2+} reduction process is concomitant with the electrocatalytic reduction of protons to H_2 catalyzed by the Co^0 electrodeposited.[48] In the reverse scan, the irreversible oxidation peak observed at −0.4 V for C/PPN^+-Co^0 (−0.5 V for C/Co^0) is ascribed to the reoxidation of the electrodeposited Co^0 to Co^{2+}, which is then dissolved in water.[26] Consequently, we chose to electrodeposit Co^0 on C and C/PPN^+ at −1.3 V, since at this potential the Co^0 electrogeneration can be promoted while minimizing H_2 generation. The Co loading (Γ_{Co}) on the C/PPN^+

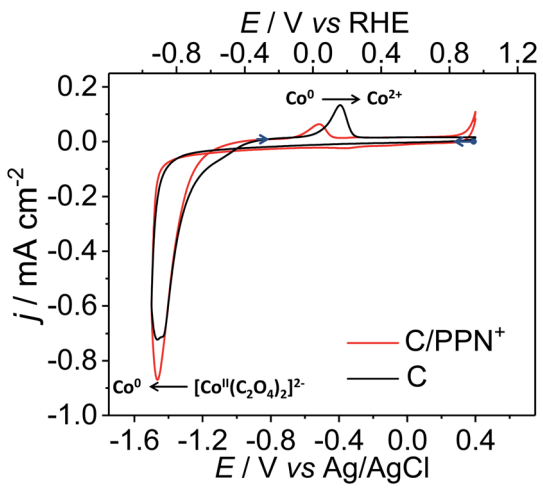

Fig. 1 Cyclic voltammetry performed at C (black line) and C/PPN^+ (Γ_{N^+} = 1.2 ± 0.1 × 10^{-7} mol cm^{-2}) (red line) electrodes (3 mm of diameter) in a 0.1 M borate buffer solution (pH 6) of 4 mM $CoSO_4$, 20 mM $Na_2C_2O_4$ and 0.1 M Na_2SO_4; the C/PPN^+ electrode was dipped in the aforementioned aqueous solution for 1 h before the cyclic voltammetry experiment.

 This journal is © The Royal Society of Chemistry 2021

Open Access Article. Published on 05 August 2021. Downloaded on 9/22/2024 5:52:21 AM.
This article is licensed under a Creative Commons Attribution-NonCommercial 3.0 Unported Licence.

and C electrodes was estimated to be 2.27 ($\pm$0.45) $\times$ 10^{-8} and 5.07 ($\pm$0.33) $\times$ 10^{-8} mol cm^{-2}, corresponding to deposition yields of 7.8 and 17.4%, respectively, calculated by ICP-MS measurements. Thus, for the same quantity of charge (4 mC), the amount of Co^0 deposited on the C/PPN$^+$ film is 2.23 times smaller than that deposited on the naked C electrode. The average Γ_{Co}/Γ_{N^+} ratio within the C/PPN$^+$-Co^0 electrodes has been determined to be 0.19, considering the average surface coverage values of Co and PPN$^+$, which are respectively Γ_{Co} = 2.27 $\times$ 10^{-8} mol cm^{-2} and Γ_{N^+} = 1.2 $\times$ 10^{-7} mol cm^{-2}.

The last step is the oxidation of Co^0 to cobalt oxide. Firstly, a partial oxidation of Co^0 to CoO occurs almost instantaneously under air exposure during the transfer of the C/PPN$^+$-Co^0 and C/Co^0 electrodes into an aqueous borate buffer solution at pH 9.2. The spontaneous air oxidation of Co^0 to CoO is well known and was previously reported by the groups of Rice[55] and Zhao.[56] Then, to oxidize CoO to higher oxidation states than II (*i.e.* to CoO_x), five consecutive cycles between 0 and +1.2 V were performed in a 0.1 M borate buffer solution (pH 9.2) (Fig. 2 and Scheme 1). The generation of cobalt oxide is evidenced by the appearance of its typical small intensity reversible Co^{II}/Co^{III} redox process[13,57,58] with anodic and cathodic peaks respectively located at +0.58 and +0.53 V for C/PPN$^+$-CoO_x, and at +0.56 and +0.51 V for C/CoO_x (Fig. 2D). Increasing the number of anodic cycles does not lead to a significant increase of the Co^{II}/Co^{III} redox process. The similarity of the Co^{II}/Co^{III} redox processes for C/PPN$^+$-CoO_x and C/CoO_x indicates that the same nature of cobalt oxide is generated on both electrodes (Fig. 2D). X-ray photoelectron spectroscopy (XPS) measurements performed on C/PPN$^+$-CoO_x after the electro-oxidation of CoO particles indeed suggest a mixture of a mixed valence cobalt oxide (Co_3O_4) and a cobalt oxyhydroxide (CoOOH) (see below). Note that a similar Co^{II}/Co^{III} redox process in the same potential range was obtained by the group of Spiccia[59] for cobalt oxide electrodeposited in a borate buffer (pH 9.2) from solutions of negatively charged cobalt complexes.

It can also be noted that in the first scan from 0 to +1.2 V of the C/PPN$^+$-CoO electrode (Fig. 2A), two broad anodic processes are observed at +0.67 and +0.95 V in the cyclic voltammogram, which correspond respectively to the oxidation and the overoxidation of polypyrrole. The mechanism of the overoxidation of polypyrrole is complex but has been well investigated.[60–62] During its overoxidation, a nucleophilic attack at α- or β-carbon of a pyrrole unit occurs, resulting in the introduction of oxygen atoms on the polymer backbone and a loss of its conductivity. After the overoxidation, the polymeric chain remains globally

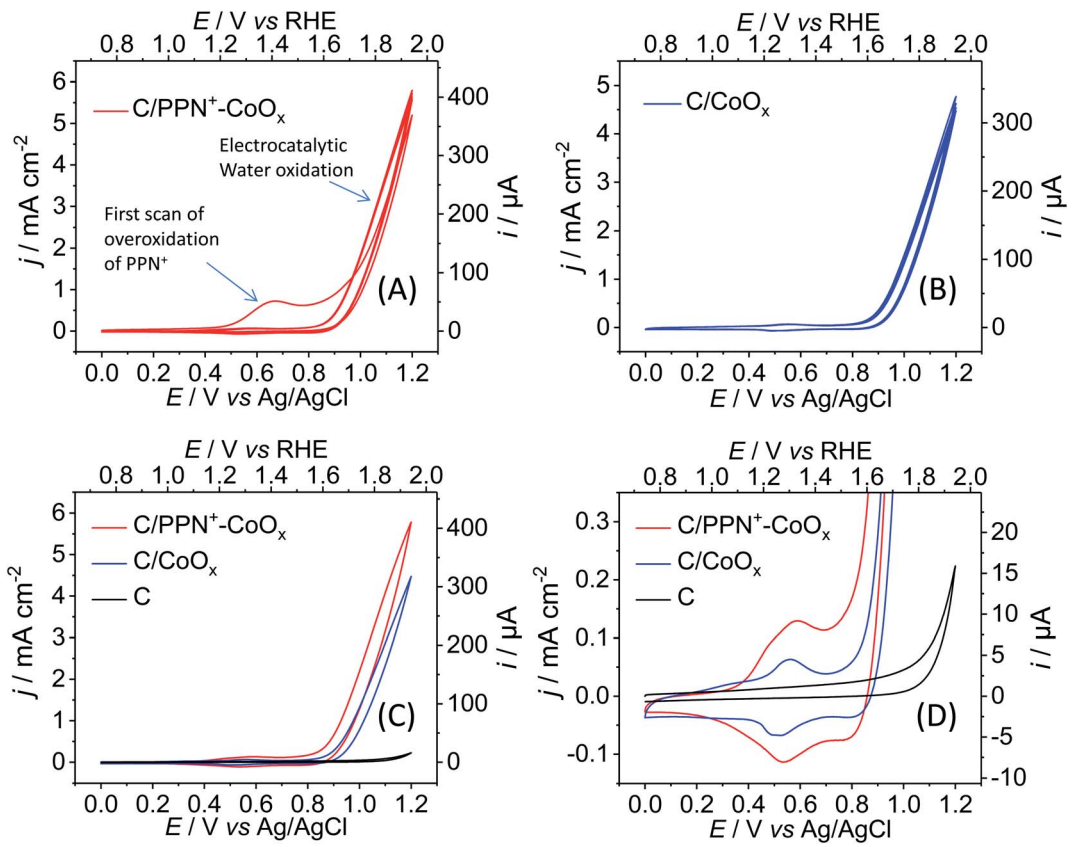

Fig. 2 Electro-induced generation of CoO_x from CoO by repeated cyclic voltammetry (CV) scans (5 consecutive scans; scan rate of 50 mV s^{-1}) in a 0.1 M borate buffer solution (pH 9.2) at (A) the C/PPN$^+$-CoO electrode (Γ_{N^+} = 1.2 $\pm$ 0.1 $\times$ 10^{-7} mol cm^{-2} and Γ_{Co} = 2.27 $\pm$ 0.45 $\times$ 10^{-8} mol cm^{-2}) and (B) the C/CoO electrode (Γ_{Co} = 5.07 $\pm$ 0.33 $\times$ 10^{-8} mol cm^{-2}). (C) Overlay of the 5th scans of the C/PPN$^+$-CoO (red) and C/CoO (blue) electrodes (in black, the electroactivity of a naked C electrode of 3 mm diameter) and (D) zoom of part (C) showing the redox process of the cobalt oxide.

Open Access Article. Published on 05 August 2021. Downloaded on 9/22/2024 5:52:21 AM.
This article is licensed under a Creative Commons Attribution-NonCommercial 3.0 Unported Licence.

intact, the ammonium substituents are still present in the film and the CoO_x particles stay embedded in the overoxidized polymer. Consequently, after the first scan, only the Co^{II}/Co^{III} redox process is observed in the CV below +0.7 V and the redox behavior of the polypyrrole has disappeared, meaning that the polymer conductivity is fully destroyed owing to its complete overoxidation. The electronic conductivity of the PPN^+-CoO_x film, which is effective for potentials above +0.3 V (Fig. 2D), is thus only ensured by the cobalt oxide nanoparticles, presumably *via* percolation, while the overoxidized PPN^+ acts as a nonconductive matrix maintaining the nanoparticles at the surface of the electrode, as we previously observed for C/PPN^+-NiO_x electrodes.[48]

The generation of the CoO_x particles on C and C/PPN^+ electrodes is quasi-concomitant with the catalytic water oxidation observed in their CVs (Fig. 2) by a growing catalytic current above +0.80 V. It is important to note that the catalytic current density (j) of the C/PPN^+-CoO_x electrode at +1.2 V is higher than that of the C/CoO_x electrode, with 5.77 *vs.* 4.76 mA cm^{-2}, respectively (Fig. 2A and B), evidencing the better catalytic performance of C/PPN^+-CoO_x in spite of the lower loading of cobalt within the polymer film. This result could be ascribed to the greater nanostructuration of the CoO_x embedded into the polymeric PPN^+ matrix. The difference of nanostructuration between C/PPN^+-CoO_x and C/CoO_x, which is related to their electrochemically active surface area, can be qualitatively estimated from their CVs. The integration of the overall current of the CVs for both electrodes between +0.3 and +0.7 V (Fig. 2D) indicates that the charge involved in the redox processes leading to the insulator/conductor conversion[63] of C/PPN^+-CoO_x as well as the Co^{II}/Co^{III} conversion of redox active sites exposed to the electrolyte[57] is 1.81 times greater than that of C/CoO_x. Given that there is 2.23 times less cobalt in C/PPN^+-CoO_x compared to C/CoO_x (see above), the electrochemically active surface area of the nanocomposite electrode is then estimated to be greater than that of the simple cobalt oxide electrode.

In order to confirm the higher nanostructuration of the composite material, the capacitance of C/PPN^+-CoO_x and C/CoO_x electrodes was estimated by electrochemical impedance spectroscopy (EIS). Indeed, the capacitance of an electrode is directly correlated with its electrochemically active surface area and thus with its structuration.[64–66] Bode phase and Nyquist plots (Fig. 3 and S5†) were recorded with both electrodes in borate buffer solution at pH 9.2 for different potentials (0.2, 0.6, 0.8, 0.9 and 1.0 V). The impedance spectra obtained were fitted with the equivalent circuit conventionally used for the catalytic oxidation of water.[13,67–69] The equivalent circuit is shown in the inset of Fig. 3C and is composed of the resistance of the electrolyte (R_s) between the working and reference electrodes, the double layer capacitance of the working electrode (C_{dl}), the electron transport resistance (R_{tr}, also called polarization resistance) of the film (*i.e.* PPN^+-CoO_x or CoO_x), and the capacitance (C_{sub}) and resistance (R_{sub}) related to the charge transfer between the cobalt oxide particle and its surface intermediates involved in the water oxidation process. For the curve fitting, we chose to replace the capacities with constant phase elements (CPEs) in order to take into account the inhomogeneity of the system, which is commonly associated with nanostructured electrodes with a high roughness factor.[69–72] The values of the equivalent circuit elements obtained by the experimental data fitting are reported in Table 1 and are averages calculated from measurements performed on three different electrodes for each film.

Three potential domains with different electrochemical behaviours for C/PPN^+-CoO_x and C/CoO_x were observed by EIS, the latter being correlated with their CVs: the regions around +0.2 V, between +0.6 and +0.8 V and above +0.9 V. At a potential of +0.2 V, the impedance spectra of C/PPN^+-CoO_x and C/CoO_x could not be correctly fitted because the impedance measured at this potential is very high and different from those of the other spectra obtained with potentials between +0.6 and +1.0 V (Fig. 3C and S5C†). Therefore only the values of the equivalent

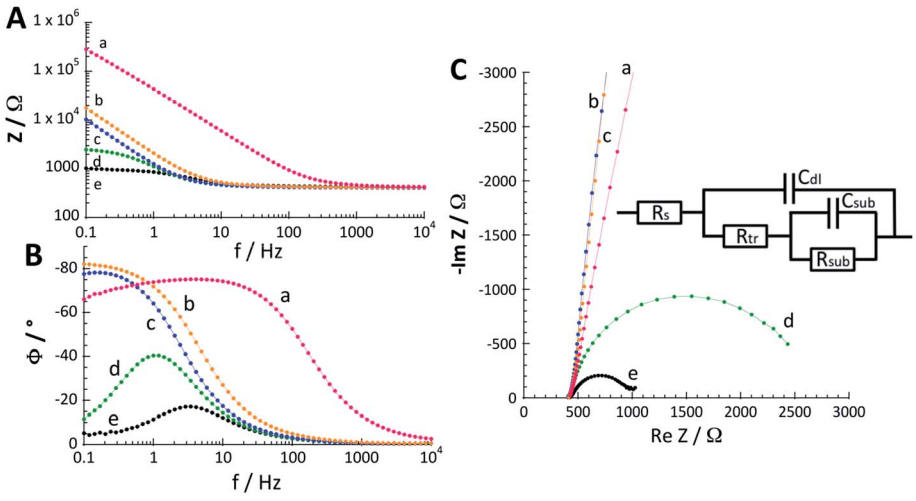

Fig. 3 Bode (module (A) and phase (B)) and Nyquist plots (C) recorded at the C/PPN^+-CoO_x ($\Gamma_{N^+} = 1.2 \pm 0.1 \times 10^{-7}$ mol cm^{-2} and $\Gamma_{Co} = 2.27 \pm 0.45 \times 10^{-8}$ mol cm^{-2}) electrode (3 mm of diameter) in a 0.1 M borate buffer solution (pH 9.2) at different potentials of 0.2 (a), 0.6 (b), 0.8 (c), 0.9 (d) and 1.0 V (e) *vs.* Ag/AgCl; inset in (C) shows the equivalent circuit model used to fit the EIS data.

 This journal is © The Royal Society of Chemistry 2021

Open Access Article. Published on 05 August 2021. Downloaded on 9/22/2024 5:52:21 AM.
This article is licensed under a Creative Commons Attribution-NonCommercial 3.0 Unported Licence.

Table 1 Values of equivalent circuit elements (R_{tr}, C_{dl}, and n_1, and R_{sub}, C_{sub}, and n_2) obtained for the fitting of the experimental data obtained for various potentials with C/PPN$^+$-CoO$_x$ and C/CoO$_x$ in a 0.1 M borate buffer at pH 9.2

E^a (V)	R_{tr} (Ω cm^{-2})	C_{dl} (mF cm^{-2})	n_1	R_{sub} (Ω cm^{-2})	C_{sub} (mF cm^{-2})	n_2
C/PPN$^+$-CoO$_x$						
0.6	12 ± 1	0.67 ± 0.06	0.936 ± 0.004	>10 (ref. 17)	—	—
0.8	10 ± 1	1.1 ± 0.1	0.930 ± 0.006	>10 (ref. 14)	—	—
0.9	7.2 ± 0.5	1.2 ± 0.1	0.89 ± 0.01	145 ± 9	1.32 ± 0.09	0.905 ± 0.006
1.0	5.6 ± 0.7	0.8 ± 0.2	0.875 ± 0.006	30 ± 1	1.4 ± 0.1	0.91 ± 0.01
C/CoO$_x$						
0.6	18 ± 1	0.15 ± 0.03	0.956 ± 0.003	>10 (ref. 17)	—	—
0.8	16 ± 1	0.30 ± 0.05	0.958 ± 0.003	>10 (ref. 15)	—	—
0.9	14 ± 1	0.38 ± 0.06	0.952 ± 0.003	350 ± 40	0.34 ± 0.06	0.922 ± 0.002
1.0	8.2 ± 0.8	0.30 ± 0.03	0.929 ± 0.007	40 ± 0.5	0.39 ± 0.07	0.901 ± 0.095

[a] Potentials are given *versus* Ag/AgCl.

circuit elements obtained between +0.6 and +1.0 V are reported in Table 1. This corroborates the fact that no redox process of cobalt is observable in the CVs of C/PPN$^+$-CoO$_x$ and C/CoO$_x$ in the region of +0.2 V (Fig. 2D) and both electrodes are mainly insulating in this potential region. Hence, EIS measurements confirm that the conductivity within the PPN$^+$-CoO$_x$ film is only ensured by the cobalt oxide particles through the various oxidation states of cobalt (*i.e.* Co^{II}/Co^{III} and Co^{III}/Co^{IV}).

In the region between +0.6 and +0.8 V, the EIS spectra allow recovery of only the C_{dl} and R_{tr} parameters which are here related to the Co^{II}/Co^{III} redox system. Since the water oxidation catalysis is weak or non-operative between +0.6 and +0.8 V, R_{sub}

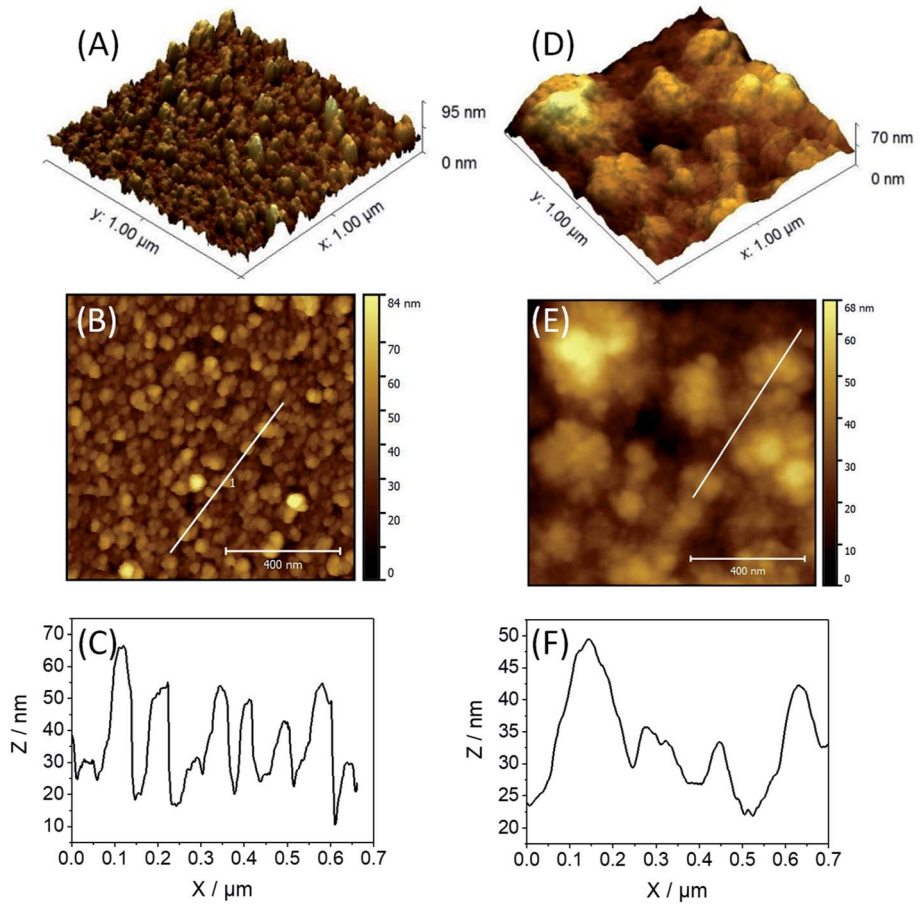

Fig. 4 3D and 2D AFM images in the peak force mode of (A and B) ITO coated with CoO$_x$ (56 mC used for the deposition of Co^0); (D and E) ITO coated with the PPN$^+$-CoO$_x$ nanocomposite (56 mC used for the deposition of PPN$^+$ and for the subsequent deposition of Co^0); (C and F) section analysis of the AFM images of ITO/CoO$_x$ and C/PPN$^+$-CoO$_x$ shown respectively in (B) and (E).

Open Access Article. Published on 05 August 2021. Downloaded on 9/22/2024 5:52:21 AM. This article is licensed under a Creative Commons Attribution-NonCommercial 3.0 Unported Licence.

and C_{sub} cannot be determined. Otherwise, EIS measurements reveal that, irrespective of the potential, the R_{tr} resistance is weaker for the C/PPN$^+$-CoO$_x$ electrode than for the C/CoO$_x$ electrode, and conversely, the C_{dl} value of C/PPN$^+$-CoO$_x$ is higher than those of C/CoO$_x$. At $^+$0.6 V in the Co(II)/Co(III) redox process (see Fig. 2D), the C_{dl} value of C/PPN$^+$-CoO$_x$ (670 μF cm^{-2}) is 4.5 times greater than that of C/CoO$_x$ (150 μF cm^{-2}). Therefore, EIS measurements confirm that C/PPN$^+$-CoO$_x$ exhibits greater nanostructuration than C/CoO$_x$. At +0.8 V, C_{dl} values drastically increase to 1100 and 300 μF cm^{-2}, respectively, for C/PPN$^+$-CoO$_x$ and C/CoO$_x$, most probably due to further oxidation of cobalt active sites leading to the onset of the OER (Fig. 2D).[13]

For potentials above +0.9 V, all the parameters of the equivalent circuit were recovered from the spectra. Indeed, the $R_{sub}C_{sub}$ loop in the equivalent circuit correctly models the interfacial charge transfer with the surface intermediates produced during the OER,[13] with the latter operating efficiently above +0.9 V. C_{dl} values are higher at +0.9 V (1200 μF cm^{-2} for C/PPN$^+$-CoO$_x$ and 380 μF cm^{-2} for C/CoO$_x$) than those at +0.6 and +0.8 V for both films for the reason mentioned above. It is worth noting that, when the potential goes from 0.9 to 1.0 V, the decrease in C_{dl} (800 μF cm^{-2} for C/PPN$^+$-CoO$_x$ and 300 μF cm^{-2} for C/CoO$_x$ at 1.0 V) was ascribed by Bisquert *et al.*[73] to the strong release of O_2 bubbles obtained at the higher potentials that diminish the electrode surface area exposed to the substrate and thus reduce its capacitive behavior. The values of n_1 and n_2 are the parameters associated with the transition from the CPE to a pure capacity.[70] When n is close to 1, it means that we are approaching a pure capacity. Here, the n values are all greater than 0.87 indicating a relatively good homogeneity[70] of both film/solution interfaces, PPN$^+$-CoO$_x$ and CoO$_x$. This may reflect the fact that the catalytic sites are certainly distributed relatively homogeneously. In addition, the n value associated with the double-layer capacitance is slightly lower for the PPN$^+$-CoO$_x$ film, which shows that in the presence of the polymer, the roughness at the film/solution interface is slightly greater. This increase in the film surface roughness was also observed by scanning electron microscopy (SEM) (see below and Fig. S7†). Therefore it can be envisaged that, even if the catalytic sites are distributed in a homogeneous manner for the two interfaces, the roughness of the polymer lowers very slightly the value of n_1. The change in this parameter would then be an illustration of the increase in the surface area of the interface provided by the roughness of the polymer, this greater surface area inducing higher catalytic activity.

2.2. Characterization of cobalt oxide and poly(pyrrole-alkylammonium) cobalt oxide nanocomposites by AFM, TEM, SEM and XPS

For atomic force microscopy (AFM), transmission electron microscopy (TEM) and scanning electron microscopy (SEM) studies, the films of PPN$^+$-CoO$_x$ or CoO$_x$ were deposited on ITO electrodes (surface of 1.0 cm^2). ITO/PPN$^+$-CoO$_x$ and ITO/CoO$_x$ electrodes were prepared with a charge of 56 mC for both the PPN$^+$ and Co^0 deposition to obtain a charge density of 56 mC cm^{-2}, similar to that used for the preparation of the C/PPN$^+$-CoO$_x$ and C/CoO$_x$ electrodes (4 mC for a C electrode with a surface of 0.071 cm^2) (see ESI† Section 3 for more details).

The surface topography of ITO/PPN$^+$-CoO$_x$ and ITO/CoO$_x$ electrodes was studied by AFM (Fig. 4). The 3D and 2D AFM images for ITO/CoO$_x$ display a homogeneous nodular topography composed of aggregated CoO$_x$ particles with a root-mean square (r.m.s.) roughness of 10.2 nm (Fig. 4A and B), while the images of ITO/PPN$^+$-CoO$_x$ exhibit an ill-defined cauliflower-like topography with a similar r.m.s. roughness of 11.6 nm (Fig. 4D and E). Such a cauliflower topology is usually observed for electrodeposited polypyrrole films.[47,48,74] From the height profile analysis of the AFM image of ITO/CoO$_x$ (Fig. 4C), the size of CoO$_x$ nodules was estimated to be 58 ± 31 nm. For ITO/PPN$^+$-CoO$_x$, nanoparticles of CoO$_x$ are buried within the PPN$^+$ film preventing the determination of the particle size by AFM. Secondary electron SEM images also confirmed the nodular and cauliflower morphologies observed for ITO/CoO$_x$ and ITO/PPN$^+$-CoO$_x$, respectively (Fig. S7†).

To further characterize the size of CoO$_x$ particles electrogenerated inside the PPN$^+$ film or directly electrodeposited on the electrode surface, the PPN$^+$-CoO$_x$ and CoO$_x$ materials were

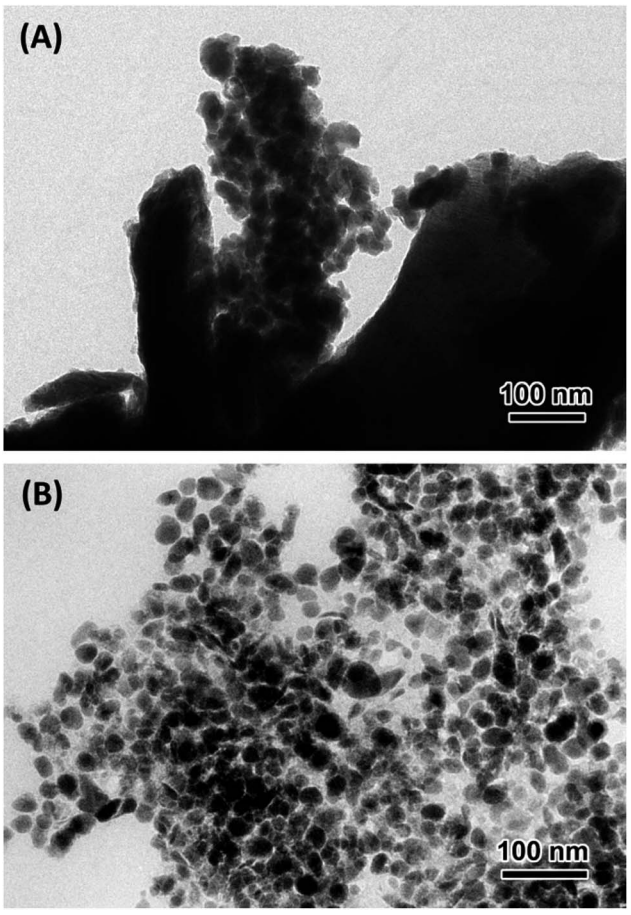

Fig. 5 TEM images of (A) CoO$_x$ (56 mC used for Co^0 deposition on ITO, scale 100 nm) and (B) PPN$^+$-CoO$_x$ nanocomposite (56 mC used for PPN$^+$ deposition and subsequent Co^0 deposition on ITO, scale 100 nm).

 This journal is © The Royal Society of Chemistry 2021

Open Access Article. Published on 05 August 2021. Downloaded on 9/22/2024 5:52:21 AM.
This article is licensed under a Creative Commons Attribution-NonCommercial 3.0 Unported Licence.

observed by TEM (Fig. 5). PPN$^+$-CoO$_x$ and CoO$_x$ fragments of films were scraped off from the ITO plates and deposited on carbon-coated copper grids. TEM images reveal large agglomerates (>100 nm) of CoO$_x$ nanoparticles for ITO/CoO$_x$ (Fig. 5A), while for ITO/PPN$^+$-CoO$_x$ the cobalt nanoparticles are not aggregated and are well-dispersed in the polymer film with an average particle size of 31 ± 20 nm (Fig. 5B). These images clearly show that the PPN$^+$ polymer prevents the nanoparticle agglomeration, resulting in a larger electrochemically active surface area of PPN$^+$-CoO$_x$ compared to that obtained from a direct electrodeposition of CoO$_x$ on the electrode surface.

The nature of the electrogenerated cobalt oxide particles within the PPN$^+$ film, after 5 cycles between 0 and +1.2 V in 0.1 M borate buffer (pH 9.2), was also studied by X-ray photoelectron spectroscopy (XPS) measurements (Fig. 6 and S6†). For XPS analysis, PPN$^+$-CoO$_x$ was electrodeposited on carbon pellets (6 mm of diameter, denoted as C_{pel}) which can be easily removed from the electrode support by unscrewing and placed in the vacuum chamber of the spectrometer (see ESI† Section 3 for their preparation and Section 10 for XPS measurement). High resolution XPS spectroscopy of the Co 2p$_{3/2}$ region reveals a broad signal, which could be deconvoluted into a series of peaks corresponding to various transitions (shake-up, plasmon loss, satellites, *etc.*) due to the complex nature of this transition metal (Fig. 6). The deconvolution of the peak at *ca.* 781 eV indicates that the cobalt deposit for the C_{pel}/PPN$^+$-CoO$_x$ anode could be a mixture of a mixed valence cobalt oxide (Co$_3$O$_4$) and a cobalt oxyhydroxide (CoOOH).[75] Foelske *et al.*[76] demonstrated by coupling electrochemical experiments with XPS measurements that poising an electrode of metallic cobalt at a potential superior to +1.18 V *vs.* Ag/AgCl in a borate buffer at pH 9.3 results in the formation of a Co$_3$O$_4$ layer on its surface. In parallel, the group of Spiccia[59] demonstrated by X-ray absorption fine structure measurements (EXAFS) that cobalt oxide, electrodeposited in a borate buffer (pH 9.2) by oxidizing a cobalt complex, closely resembles the heterogeneous CoOOH phase. Given the similarities between our study and that of Spiccia[59] in the electrochemical behavior of CoO$_x$ in borate buffer at the same pH 9.2 (see discussion above), as well as with the study of Foelske[76] in the electrogeneration of CoO$_x$ from Co^0 in borate buffer, we can assume that our cobalt oxide within PPN$^+$ could indeed contain a mixture of both Co$_3$O$_4$ and CoOOH species.

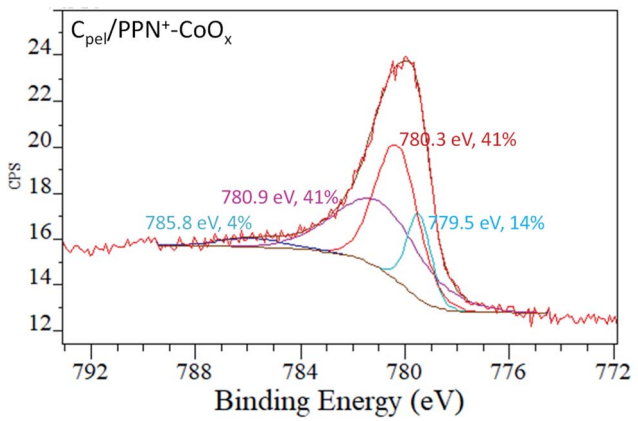

Fig. 6 XPS spectra (Co 2p$_{3/2}$ region) of the electrode surfaces of C_{pel}/PPN$^+$-CoO$_x$ after 5 cycles between 0 and +1.2 V *vs.* Ag/AgCl in a 0.1 M borate buffer (pH 9.2).

2.3. Electrocatalytic performance of cobalt oxide and poly(pyrrole-alkylammonium) cobalt oxide nanocomposite electrodes

The electrocatalytic activity of C/PPN$^+$-CoO$_x$ and C/CoO$_x$ electrodes has been investigated by cyclic voltammetry under mild basic conditions in a borate buffer solution at pH 9.2 (Fig. 2). Table 2 summarizes the catalytic OER performance of these modified electrodes and that of C/PPN$^+$-NiO$_x$ recently reported by our group[48] in a 0.1 M borate buffer solution at pH 9.2 together with those of cobalt oxide-based electrodes reported in the literature in a similar medium. In all reported cases, cobalt oxide was electrogenerated on the surface of fluorine doped tin oxide electrodes (FTO). Developing electrolyzers operating at nearly neutral pH, such as pH 9.2, is of utmost importance in view of avoiding the corrosion issue under strongly acidic or alkaline conditions.[11] Herein, the C/PPN$^+$-CoO$_x$ anode exhibits a j value of 4.04 mA cm^{-2} at a η of +0.61 V and a η value of +0.44 V at 1 mA cm^{-2} with a cobalt mass loading of 1.34 μg cm^{-2}. This performance places our nanocomposite anode among the best reported cobalt oxide-based anodes for water oxidation operating in a 0.1 M borate buffer solution at pH 9.2.

For comparison, the C/CoO$_x$ anode presents a j value of 3.40 mA cm^{-2} at a η of +0.61 V and a η value of +0.46 V at 1 mA cm^{-2} with a cobalt mass loading of 2.99 μg cm^{-2}. The C/PPN$^+$-CoO$_x$ nanocomposite electrode presents a higher j and a lower η values compared to those of C/CoO$_x$ with ~2.2 times less cobalt loading, demonstrating the beneficial effect of using a poly(pyrrole-alkylammonium) matrix to enhance the nanostructuration of the electrode material and thus its electrocatalytic performance. Of note, in the three compartment cell, the resistance R between the anode (*i.e.* the working electrode) and the Ag/AgCl reference, which causes the ohmic drop (related to the iR value) in the cell, could be different between C/PPN$^+$-CoO$_x$ and C/CoO$_x$, making the comparison of their electrocatalytic performance unfair. In view of suppressing the ohmic drop and making a fair comparison, the resistance R in the cell has been determined to be 1 and 4.6 Ω respectively with C/PPN$^+$-CoO$_x$ and C/CoO$_x$. Since these R values are low, the CVs and the catalytic current density of both electrodes are weakly affected by the iR correction (see in the ESI the CVs with and without iR correction; Fig. S2†), which means that the previous comparison of the catalytic activities of both anodes was correct. According to TEM images and EIS measurements, C/PPN$^+$-CoO$_x$ contains small CoO$_x$ particles (31 nm) with a capacitance of 670 μF cm^{-2}, while C/CoO$_x$ exhibits big agglomerates of CoO$_x$ particles (>100 nm) associated with a lower capacitance of 150 μF cm^{-2} (see above). Hence the higher catalytic activity of the C/PPN$^+$-CoO$_x$ nanocomposite compared to the direct deposition C/CoO$_x$ can be directly correlated with a greater nanostructuration of the nanocomposite that increases the electrochemically active surface

Open Access Article. Published on 05 August 2021. Downloaded on 9/22/2024 5:52:21 AM. This article is licensed under a Creative Commons Attribution-NonCommercial 3.0 Unported Licence.

Table 2 OER performances of C/PPN$^+$-CoO_x and C/CoO_x anodes prepared in this work compared to those of C/PPN$^+$-NiO_x and FTO/CoO_x anodes previously reported with a 0.1 M borate buffer solution at pH 9.2

Catalyst/electrode	j (mA cm^{-2})@η (V)	η (V)@j (mA cm^{-2})	Metal mass loading (μg cm^{-2})	Mass activity (A mg^{-1})@η (V)	TOF_{min} (s^{-1})@η (V)	Author *et al.* (ref.)
C/PPN$^+$-CoO_x	4.04@0.61	0.44@1	1.34	3.01@0.61	0.46@0.61	This work
C/PPN$^+$-CoO_x	2.17@0.51		1.34	1.62@0.51	0.25@0.51	This work
C/PPN$^+$-CoO_x	0.53@0.40		1.34	0.40@0.40	0.06@0.40	This work
C/CoO_x	3.40@0.61	0.46@1	2.99	1.14@0.61	0.17@0.61	This work
C/CoO_x	1.32@0.51		2.99	0.44@0.51	0.07@0.51	This work
C/CoO_x	0.22@0.40		2.99	0.07@0.40	0.01@0.40	This work
C/PPN$^+$-NiO_x	2.17@0.61	0.51@1	1.9	1.12@0.61	0.17@0.61	Fortage[48]
FTO/CoO_x	2.89[a]@0.51	0.37[a]@1	nd	nd	nd	Nocera[24]
FTO/CoO_x	0.41@0.40	0.53@1	46.0	0.009[b]@0.40	0.001[b]@0.40	Nocera[28]
FTO/CoO_x	1.90[a]@0.61	0.51[a]@1	1.11	1.71[b]@0.61	0.26[b]@0.61	Spiccia[59]
FTO/CoO_x	0.39[a]@0.61	0.75[a]@1	0.003	130[b]@0.61	20@0.61	Sun[79]
FTO/CoO_x	2.60[c]@0.61	nd	nd	nd	nd	Du[77]
FTO/CoO_x	1.40[c]@0.61	0.51[a]@1	3.53	0.40[b]@0.61	0.06[b]@0.61	Du[78]

[a] Values were extrapolated from the cyclic voltammograms reported by the authors. [b] Data non calculated by the authors but estimated herein from the current density (j) at defined overpotentials (η) and the mass loading of Co given in the article. [c] The current density was measured from cyclic voltammetry corrected for the ohmic drop.
nd: not determined. FTO: fluorine doped tin oxide electrode.

area of the anode and ensures a great accessibility of the active catalytic sites towards substrates such as water or OH^- ions. The higher values of mass activity and turnover frequency (TOF) of C/PPN$^+$-CoO_x (3.01 A mg^{-1} and 0.46 s^{-1}) compared to those of C/CoO_x (1.14 A mg^{-1} and 0.17 s^{-1}) at pH 9.2 at an overpotential of 0.61 V confirm the higher OER catalytic activity of the nanocomposite PPN$^+$-CoO_x material (Table 2). In order to facilitate the comparison with the electrocatalytic performance of previously reported anodes based on cobalt oxide operating at pH 9.2 with a 0.1 M borate buffer (Table 2), the CVs of C/PPN$^+$-CoO_x have been recorded at different scan rates between 5 and 100 mV s^{-1} (Fig. S3†), since various scan rates have been used to measure the performance of the reported anodes. The CVs of C/PPN$^+$-CoO_x are weakly impacted by the scan rate value, indicating that the diffusion of the borate buffer in the polypyrrole film is efficient. In other words, the electrocatalytic activity of C/PPN$^+$-CoO_x measured with a scan rate of 50 mV s^{-1} is reliable to make a fair comparison with those of the reported anodes. It appears that the mass activity and TOF values of the C/PPN$^+$-CoO_x electrode are among the highest in the literature (Table 2). Otherwise, although the CoO_x films of the literature have been realized with the same range of mass loadings (1–4 μg cm^{-2}) as that of the PPN$^+$-CoO_x nanocomposite, the comparison of the performances of these anodes is not easy and could be erroneous due to the fact all the oxide deposits reported in Table 2 were made on an FTO electrode (*i.e.* fluorine tin oxide) as a conductive support, whose conductivity is lower than that of a carbon electrode, thus possibly decreasing the overall performance of the anodes. Otherwise, it is worth noting that the comparison of the electrocatalytic activities of anodes, for which the ohmic drop correction is applied, such as those reported by Du[77,78] in Table 2, is relevant. One can see that the catalytic currents of C/PPN$^+$-CoO_x and C/CoO_x (respectively 4.04 and 3.40 mA cm^{-2} at $\eta = 0.61$ V) are higher than those of the FTO/CoO_x anodes (2.60 and 1.40 mA cm^{-2} at $\eta = 0.61$ V),[77,78] in spite of the *iR* correction and the higher cobalt loading on FTO/CoO_x in ref. 78 (3.53 μg cm^{-2} *vs.* 1.34 and 2.99 μg cm^{-2} for C/PPN$^+$-CoO_x and C/CoO_x respectively). It is also interesting to note that the OER performance of C/PPN$^+$-CoO_x is greater than that of the analogous C/PPN$^+$-NiO_x previously reported by our group,[48] which displays lower values of j (2.17 mA cm^{-2}), mass activity (1.12 A mg^{-1}) and TOF (0.17 s^{-1}) for an overpotential of 0.61 V. If we consider a similar nanostructuration for C/PPN$^+$-CoO_x and C/PPN$^+$-NiO_x anodes (particle sizes of CoO_x and NiO_x (ref. 48) within PPN$^+$ of 31 and 21 nm, respectively) and a lower metal loading of cobalt compared to that of nickel ($\Gamma_{Co} \sim 23$ nmol cm^{-2} *vs.* $\Gamma_{Ni} \sim 33$ nmol cm^{-2}),[48] CoO_x particles display a higher intrinsic catalytic activity than NiO_x for water oxidation in borate buffer at pH 9.2.

The stability of C/PPN$^+$-CoO_x and C/CoO_x electrodes at pH 9.2 in a 0.1 M borate buffer was evaluated by chronoamperometry measurements over a period of about 2 h at an applied potential of +1.2 V *vs.* Ag/AgCl (Fig. 7). The current density of the C/CoO_x electrode decreases from 6 to 5.30 mA cm^{-2} after 5 min of electrolysis and then gradually decreases to reach a pseudo-plateau at 4.90 mA cm^{-2} after 2.5 h of electrolysis. Meanwhile the current density of C/PPN$^+$-CoO_x increases during the first hour from 7.16 to 7.80 mA cm^{-2} and then gradually decreases to reach a pseudo-plateau at 7.00 mA cm^{-2} after 2.5 h of electrolysis. Over this time range, the catalytic current of C/PPN$^+$-CoO_x is relatively stable and 1.43 times higher than that of C/CoO_x, even though there is 2.2 times less cobalt in the former. Once again, this demonstrates the superiority of the nanocomposite electrode over a simple Co-based electrode.

Unfortunately, the current density of C/PPN$^+$-CoO_x decreases suddenly and drastically after 2.5 h of electrolysis reaching 2.36 mA cm^{-2} after 6 h of electrolysis, whereas the current density of C/CoO_x decreases slowly until 4.3 mA cm^{-2} over the same period of time. As we previously observed for the C/PPN$^+$-NiO_x

 This journal is © The Royal Society of Chemistry 2021

Open Access Article. Published on 05 August 2021. Downloaded on 9/22/2024 5:52:21 AM.
This article is licensed under a Creative Commons Attribution-NonCommercial 3.0 Unported Licence.

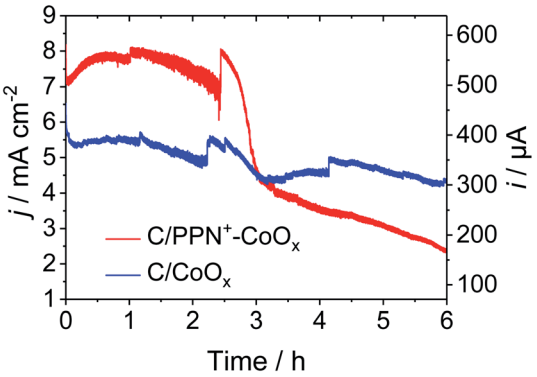

Fig. 7 Chronoamperograms recorded at the C/PPN$^+$-CoO$_x$ ($\Gamma_{N^+} = 1.2 \pm 0.1 \times 10^{-7}$ mol cm^{-2} and $\Gamma_{Co} = 2.27 \pm 0.45 \times 10^{-8}$ mol cm^{-2}) and C/CoO$_x$ ($\Gamma_{Co} = 5.07 \pm 0.33 \times 10^{-8}$ mol cm^{-2}) electrodes (3 mm of diameter) in a 0.1 M borate buffer solution (pH 9.2), at a constant potential of +1.2 V *vs.* Ag/AgCl under stirring.

anode,[48] the decrease of catalytic current with C/PPN$^+$-CoO$_x$ is not due to the decomposition of the material or to the gradual release of cobalt oxide particles but to the partial film detachment from the carbon electrode induced by the oxygen bubbles released during the electrolysis (see in Picture S1 in the ESI,† the view of a C/PPN$^+$-CoO$_x$ electrode before and after the electrolysis for 6 h, and the view of the PPN$^+$-CoO$_x$ film floating in the borate electrolyte after its partial detachment from the C electrode induced by the electrolysis). Note that the relatively good stability of C/CoO$_x$ (*i.e.* without PPN$^+$) could be ascribed to the good physisorption of the cobalt oxide on the carbon electrode and also to the self-healing phenomenon occurring during electrocatalytic water oxidation with cobalt oxide in a borate buffer.[25,80,81]

To avoid the film detachment from the electrode surface under prolonged electrolysis at +1.2 V, the physisorption of the polypyrrole film on the electrode has been increased by the electrodeposition of the PPN$^+$-CoO$_x$ material on a carbon paper electrode (denoted as C_{pap}) with a high roughness and a larger surface of 2.4 cm^2, following the same procedure used for the preparation of the PPN$^+$-CoO$_x$ nanocomposite on a small glassy carbon electrode (see Section 3 in the ESI for its preparation and Fig. S4A†). The deposition of the PPN$^+$-CoO$_x$ film on the C_{pap} electrode was evidenced by SEM images (Fig. 8A and B) and EDX spectroscopy (Fig. 8C) by comparison with a pristine C_{pap} electrode (Fig. S8†). The EDX spectrum of C_{pap} exhibits only the characteristic peaks of C and O atoms respectively at 0.28 and 0.50 keV (Fig. S8C†), while the EDX spectrum of C/PPN$^+$-CoO$_x$ displays broader peaks below 0.6 keV ascribed to the C, N and O atoms of the overoxidized polypyrrole film, in addition to the C/O peaks of C_{pap} (see above), along with the typical peaks of cobalt at 0.78 (Lα) and 6.92 keV (Kα) (Fig. 8C). As observed above on the CV of C/PPN$^+$-CoO$_x$ recorded in a borate buffer at pH 9.2 (Fig. 2), C_{pap}/PPN$^+$-CoO$_x$ displays the redox signature of Co^{II}/Co^{III} between 0.3 and 0.8 V *vs.* Ag/AgCl with a strong catalytic current attributed to water oxidation to O$_2$, reaching 3.6 mA cm^{-2} at 1.2 V *vs.* Ag/AgCl (Fig. 9 and S4†). Otherwise, on this rough support, no PPN$^+$-CoO$_x$ film detachment is observed and

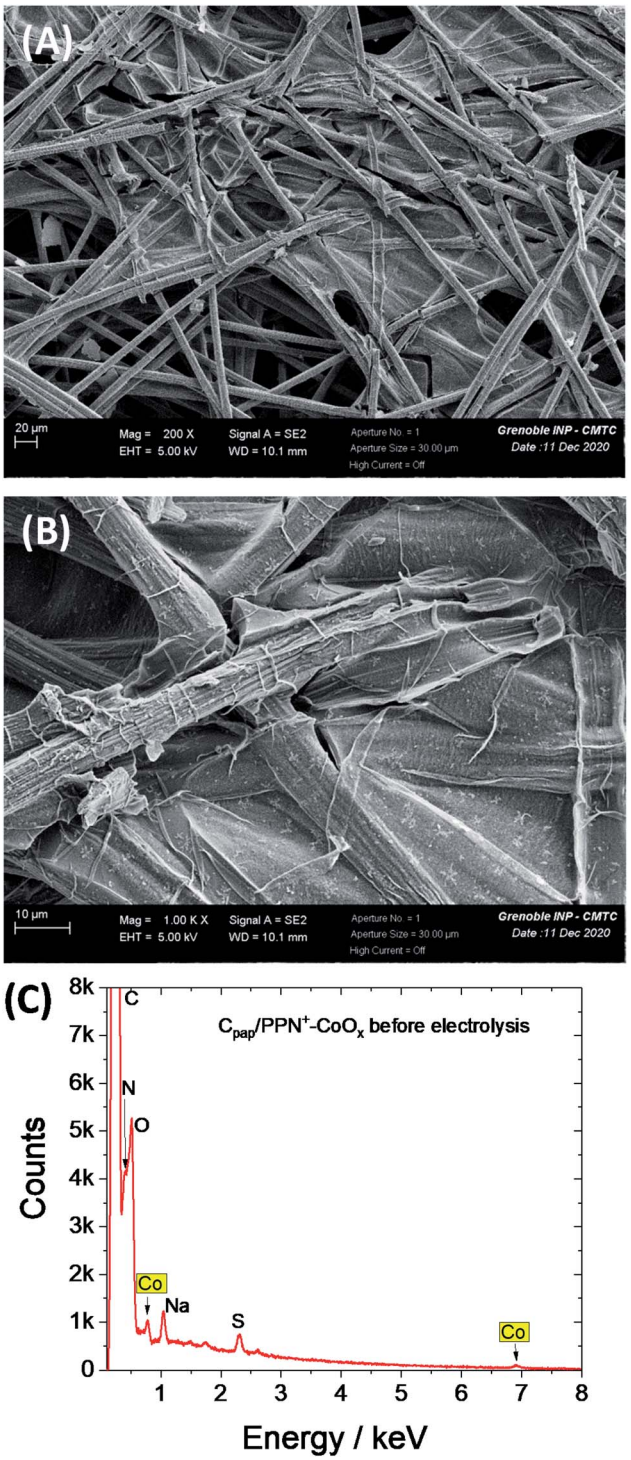

Fig. 8 SEM images of the C_{pap}/PPN$^+$-CoO$_x$ electrode at (A) 200× magnification and (B) 1000× magnification and (C) corresponding EDX spectrum.

the catalytic current of C_{pap}/PPN$^+$-CoO$_x$ is stable over 43 h of electrolysis at a constant potential of +1.2 V *vs.* Ag/AgCl in a borate buffer at pH 9.2 (Fig. 10). In addition, the stability of the catalytic current is a good indication of the stability of the CoO$_x$ nanoparticles which remain embedded in the PPN$^+$ film during electrocatalysis. This is confirmed by the post-

Open Access Article. Published on 05 August 2021. Downloaded on 9/22/2024 5:52:21 AM.
This article is licensed under a Creative Commons Attribution-NonCommercial 3.0 Unported Licence.

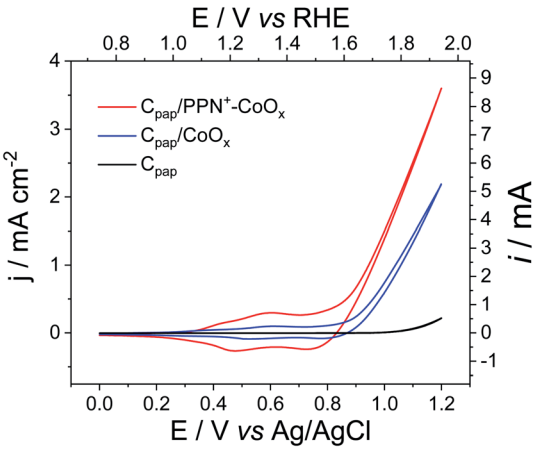

Fig. 9 Cyclic voltammograms recorded at C_{pap}/PPN^+-CoO_x (red, $\Gamma_{N^+} = 1.53 \pm 0.03 \times 10^{-7}$ mol cm^{-2} and $\Gamma_{Co} = 1.04 \pm 0.16 \times 10^{-8}$ mol cm^{-2}), C_{pap}/CoO_x (blue, $\Gamma_{Co} = 3.70 \pm 0.27 \times 10^{-8}$ mol cm^{-2}) and C_{pap} (black) electrodes (2.4 cm^2) in a 0.1 M borate buffer solution (pH 9.2); scan rate of 50 mV s^{-1}.

electrolysis characterizations of the PPN^+-CoO_x material deposited on C_{pap}.

Indeed, the stability of the film on C_{pap} allows us to perform post-electrolysis characterization by SEM and EDX on this electrode material. Post-electrolysis characterization on ITO electrodes was not possible due to the detachment of the PPN^+-CoO_x film under electrolysis at +1.2 V. The SEM images and EDX spectra of C_{pap}/PPN^+-CoO_x before (Fig. 8) and after 43 h of electrolysis (Fig. 11 and 12) are very similar. The EDX spectra exhibit the same signals with similar intensity for the C/N/O peaks below 0.6 keV and for cobalt at 0.78 and 6.92 keV (Fig. 12). This result strongly indicates that the overoxidized PPN^+ film and the embedded CoO_x nanoparticles remain unchanged even after being maintained at +1.2 V *vs.* Ag/AgCl in a borate buffer at pH 9.2 over such a long period of time. The PPN^+ film thus imparts a great stability to the nanocomposite material by

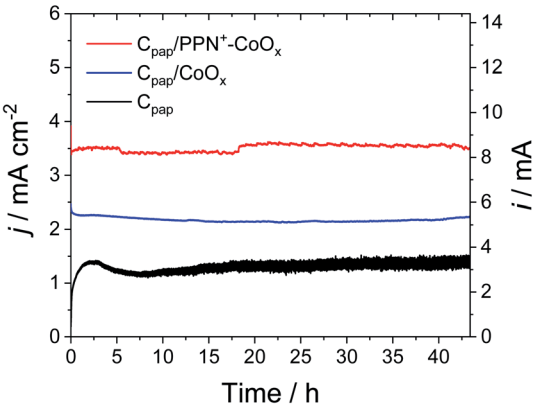

Fig. 10 Chronoamperograms recorded at C_{pap}/PPN^+-CoO_x (red, $\Gamma_{N^+} = 1.53 \pm 0.03 \times 10^{-7}$ mol cm^{-2} and $\Gamma_{Co} = 1.04 \pm 0.16 \times 10^{-8}$ mol cm^{-2}), C_{pap}/CoO_x (blue, $\Gamma_{Co} = 3.70 \pm 0.27 \times 10^{-8}$ mol cm^{-2}) and C_{pap} (black) electrodes (2.4 cm^2) in a 0.1 M borate buffer solution (pH 9.2) at a constant potential of +1.2 V *vs.* Ag/AgCl maintained for *ca.* 43 h under stirring.

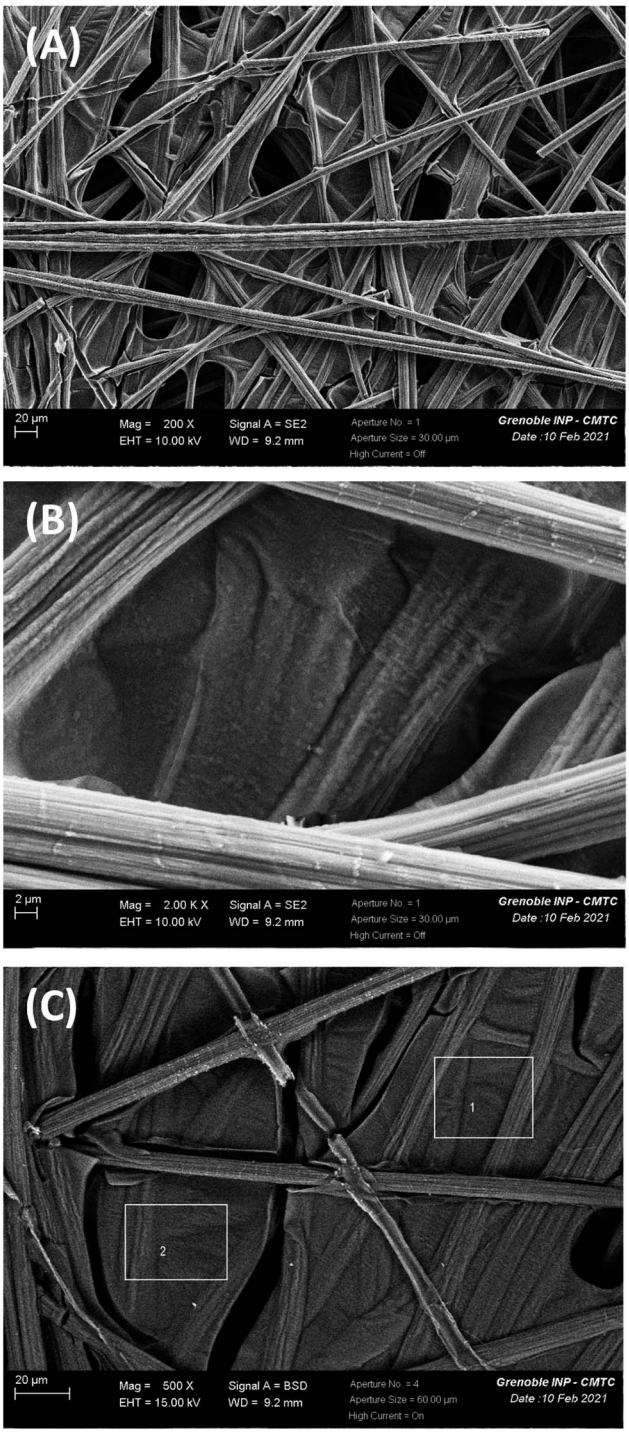

Fig. 11 SEM image of the C_{pap}/PPN^+-CoO_x electrode: (A) 200× magnification, (B) 2000× magnification and (C) 500× magnification, along with zones 1 and 2 for which EDX analysis (see below Fig. 12) has been performed on the C_{pap}/PPN^+-CoO_x electrode after electrolysis for 43 h at 1.2 V *vs.* Ag/AgCl in a 0.1 M borate buffer (pH 9.2).

preventing the corrosion and the degradation of CoO_x nanoparticles, in addition to the phenomenon of self-healing that is known for cobalt oxide in a borate buffer.[25,80,81] We also verified the formation of oxygen by gas chromatography. A high faradaic yield of 97% towards O_2 evolution was measured after 2 h of

 This journal is © The Royal Society of Chemistry 2021

Open Access Article. Published on 05 August 2021. Downloaded on 9/22/2024 5:52:21 AM.
This article is licensed under a Creative Commons Attribution-NonCommercial 3.0 Unported Licence.

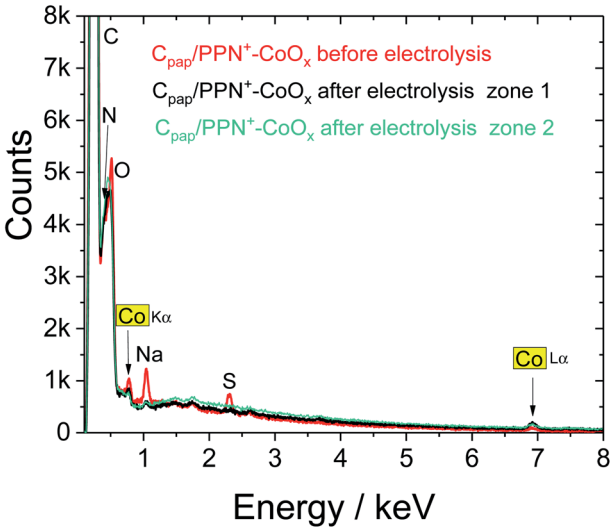

Fig. 12 EDX spectra of the SEM images respectively in Fig. 11 of C_{pap}/PPN$^+$-CoO_x before (red) and after electrolysis for 43 h at +1.2 V *vs.* Ag/AgCl in a 0.1 M borate buffer (pH 9.2) performed in zone 1 (black) and in zone 2 (green).

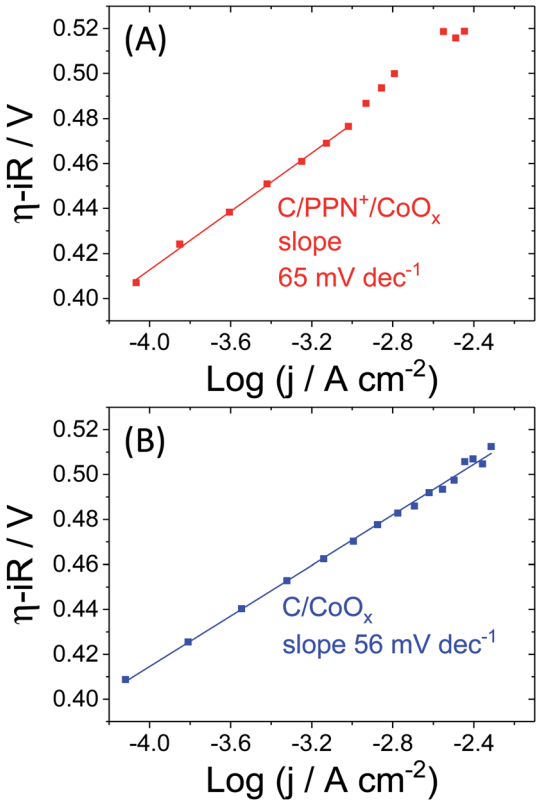

Fig. 13 Tafel plots recorded at the C/PPN$^+$-CoO_x ($\Gamma_{N^+} = 1.2 \pm 0.1 \times 10^{-7}$ mol cm^{-2} and $\Gamma_{Co} = 2.27 \pm 0.45 \times 10^{-8}$ mol cm^{-2}) (A) and C/CoO_x ($\Gamma_{Co} = 5.07 \pm 0.33 \times 10^{-8}$ mol cm^{-2}) (B) rotating disc electrodes (3 mm of diameter) in a 0.1 M borate buffer solution (pH 9.2) under rotation (1200 rpm).

electrolysis (see ESI† Section 12), confirming that C_{pap}/PPN$^+$-CoO_x is an efficient and selective anode for water oxidation to O_2.

To compare the performance of the PPN$^+$-CoO_x nanocomposite with that of a simple CoO_x film, CoO_x was also electrodeposited on the rough C_{pap} electrode (without PPN$^+$). The CV of C_{pap}/CoO_x exhibits a similar Co^{II}/Co^{III} signature between 0.3 and 0.8 V *vs.* Ag/AgCl, but despite a cobalt loading 3.5 times higher ($3.70 \pm 0.27 \times 10^{-8}$ mol cm^{-2}) than that on C_{pap}/PPN$^+$ ($1.04 \pm 0.16 \times 10^{-8}$ mol cm^{-2}), the corresponding catalytic current density of 2.37 mA cm^{-2} at 1.2 V remains lower than that of C_{pap}/PPN$^+$-CoO_x (3.61 mA cm^{-2}) (Fig. 9 and S4†), further demonstrating the benefits of using PPN$^+$ films. It is interesting to note that, after a long electrolysis for 43 h at 1.2 V *vs.* Ag/AgCl in a borate buffer at pH 9.2, the catalytic current of C_{pap}/CoO_x is also very stable (Fig. 10) as previously observed on a small carbon electrode with C/CoO_x, most probably due to the self-healing phenomenon.[25]

To obtain some mechanistic information, Tafel analysis was performed through stepwise chronoamperometry at pH 9.2 on C/PPN$^+$-CoO_x and C/CoO_x electrodes (Fig. 13, see Section 7 in the ESI for more details†). A Tafel slope value of 56 mV dec^{-1} was determined for C/CoO_x corresponding to a fast equilibrated electron transfer. The catalytic process is thus not controlled by an electron transfer but by a chemical step following this electron transfer.[13,26,82] Similar values were reported with cobalt oxide catalysts in borate buffer at pH 9.2 by several groups such as those of Nocera,[28] Du[77,78] and Spiccia.[59] For C/PPN$^+$-CoO_x, a Tafel slope of 65 mV dec^{-1}, close to that of C/CoO_x, was estimated within a region of corrected overpotentials between +0.41 and +0.47 V (*i.e.* within a potential region between +0.9 and +1.02 V *vs.* Ag/AgCl). Above +0.47 V, the Tafel plot of C/PPN$^+$-CoO_x deviates from linearity most probably due to the limitations by mass transport of the buffer within the polypyrrole film, which could not be easily obviated by the rotation of the electrode.[83] However, the similar Tafel slopes of C/PPN$^+$-CoO_x and C/CoO_x confirm that the O_2 evolution occurring with these two electrodes involves the same catalytic mechanism.

3. Conclusion

We prepared a very efficient OER anode material based on a cobalt oxide-poly(pyrrole-alkylammonium) nanocomposite deposited on an electrode surface by an easy all-electrochemical procedure. TEM images and EIS measurements evidenced the high nanostructuration of the PPN$^+$-CoO_x nanocomposite owing to the small CoO_x nanoparticles of *ca.* 30 nm well dispersed and not aggregated in the polypyrrole film. The nature of the cobalt oxide has also been identified by XPS as potentially being a mixture of Co_3O_4/CoOOH. By comparison with CoO_x directly deposited on an electrode surface (CoO_x particles > 100 nm), we demonstrated that the high nanostructuration of the composite material is the origin of the higher OER electrocatalytic performances. The nanocomposite material exhibits an exceptional mass activity of 3.01 A mg^{-1} and TOF values of 0.46 s^{-1} along with a faradaic yield of 97% for water oxidation at mildly basic pH 9.2 at an overpotential of 0.61 V, and a Tafel slope of 65 mV dec^{-1}. The cobalt oxide–polypyrrole nanocomposite electrode is among the most efficient

Open Access Article. Published on 05 August 2021. Downloaded on 9/22/2024 5:52:21 AM.
This article is licensed under a Creative Commons Attribution-NonCommercial 3.0 Unported Licence.

cobalt oxide-based anodes previously reported operating in a 0.1 M borate buffer solution at pH 9.2, but it also outperforms cobalt oxide electrogenerated on a naked electrode surface by the same electrochemical procedure. In addition, when the PPN^+-CoO_x material is electrodeposited on a rough carbon paper, the physisorption of the nanocomposite film is considerably enhanced and consequently its catalytic activity is very stable beyond 43 h of electrolysis. Post-electrolysis characterization by SEM and EDX also confirms the integrity of the PPN^+-CoO_x material after many hours of electrocatalysis. This work demonstrates the beneficial role of a positively charged polypyrrole matrix in the preparation of small particles of cobalt oxide and in the achievement of a highly stable and active anode for water oxidation. The elaboration of such a polypyrrole-metal oxide nanocomposite material could be easily extended to other abundant first-row transition metals such as manganese and iron, and also could be useful to prepare mixed metal oxides such as $NiFeO_x$ or $CoFeO_x$, which are the most efficient OER catalysts under alkaline or mildly basic conditions.

Conflicts of interest

There are no conflicts to declare.

Acknowledgements

ANID (ex Becas-Chile-Conicyt) "Programa de formación de capital humano avanzado" for the PhD fellowship of D. V. M. (No. 72150091) and C. N. A. (No. 72170399), ANID/FONDECYT Postdoctoral project of D. V. M. (Grant No. 3200467), "Université Grenobles Alpes" for the PhD fellowship of B. D., The CMTC platform of "Institut Poolythechinique de Grenoble" for SEM-EDX measurements, the NanoBio-ICMG Platform (UAR 2607, Grenoble) for granting access to the Electron Microscopy facility, the ECOS-CONICYT exchange program (C13E01), Ministères de l'Europe et des Affaires Etrangères (MEAE) et de l'Enseignement Supérieur, de la Recherche et de l'Innovation (MESRI) (PHC Brancusi program (43546QA)) and the COST CM1202 program (PERSPECT H_2O) are acknowledged. This work has been partially supported by LabEx Arcane and CBH-EUR-GS (ANR-17-EURE-0003).

References

1 A. A. Gewirth and M. S. Thorum, *Inorg. Chem.*, 2010, **49**, 3557.
2 O. Z. Sharaf and M. F. Orhan, *Renew. Sustain. Energy Rev.*, 2014, **32**, 810.
3 N. Armaroli and V. Balzani, *ChemSusChem*, 2011, **4**, 21.
4 T. R. Cook, D. K. Dogutan, S. Y. Reece, Y. Surendranath, T. S. Teets and D. G. Nocera, *Chem. Rev.*, 2010, **110**, 6474.
5 F. Ausfelder and A. Bazzanella, in *Hydrogen Science and Engineering: Materials, Processes, Systems and Technology*, ed. D. Stolten and B. Emonts, Wiley-VCH, 2016, vol. 1, p. 19.
6 K. Ayers, N. Danilovic, R. Ouimet, M. Carmo, B. Pivovar and M. Bornstein, *Annu Rev Chem Biomol*, 2019, **10**, 219.
7 K. E. Ayers, E. B. Anderson, C. B. Capuano, B. D. Carter, L. T. Dalton, G. Hanlon, J. Manco and M. Niedzwiecki, *ECS Trans.*, 2010, **33**, 3.
8 J. Mergel, D. L. Fritz and M. Carmo, in *Hydrogen Science and Engineering : Materials, Processes, Systems and Technology*, ed. D. Stolten and B. Emonts, Wiley-VCH, 2016, vol. 1, p. 331.
9 D. Zhang and K. Zeng, in *Hydrogen Science and Engineering : Materials, Processes, Systems and Technology*, ed. D. Stolten and B. Emonts, Wiley-VCH, 2016, vol. 1, p. 283.
10 G. Gahleitner, *Int. J. Hydrogen Energy*, 2013, **38**, 2039.
11 P. Li, R. Zhao, H. Chen, H. Wang, P. Wei, H. Huang, Q. Liu, T. Li, X. Shi, Y. Zhang, M. Liu and X. Sun, *Small*, 2019, **15**, 1805103.
12 J. O. M. Bockris, *J. Chem. Phys.*, 1956, **24**, 817.
13 R. L. Doyle, I. J. Godwin, M. P. Brandon and M. E. G. Lyons, *PhysChemChemPhys*, 2013, **15**, 13737.
14 M. D. Kärkäs, O. Verho, E. V. Johnston and B. Åkermark, *Chem. Rev.*, 2014, **114**, 11863.
15 J. D. Blakemore, R. H. Crabtree and G. W. Brudvig, *Chem. Rev.*, 2015, **115**, 12974.
16 P. Benson, G. W. D. Briggs and W. F. K. Wynne-Jones, *Electrochim. Acta*, 1964, **9**, 281.
17 V. Y. Shafirovich and V. V. Strelets, *Nouv. J. Chim.*, 1978, **2**, 199.
18 S. M. Jasem and A. C. C. Tseung, *J. Electrochem. Soc.*, 1979, **126**, 1353.
19 L. D. Burke, M. E. Lyons and O. J. Murphy, *J. Electroanal. Chem.*, 1982, **132**, 247.
20 Y. W. D. Chen and R. N. Noufi, *J. Electrochem. Soc.*, 1984, **131**, 731.
21 S. P. Jiang and A. C. C. Tseung, *J. Electrochem. Soc.*, 1991, **138**, 1216.
22 E. B. Castro, C. A. Gervasi and J. R. Vilche, *J. Appl. Electrochem.*, 1998, **28**, 835.
23 M. W. Kanan and D. G. Nocera, *Science*, 2008, **321**, 1072.
24 Y. Surendranath, M. Dinca and D. G. Nocera, *J. Am. Chem. Soc.*, 2009, **131**, 2615.
25 D. A. Lutterman, Y. Surendranath and D. G. Nocera, *J. Am. Chem. Soc.*, 2009, **131**, 3838.
26 Y. Surendranath, M. W. Kanan and D. G. Nocera, *J. Am. Chem. Soc.*, 2010, **132**, 16501.
27 M. W. Kanan, J. Yano, Y. Surendranath, M. Dinca, V. K. Yachandra and D. G. Nocera, *J. Am. Chem. Soc.*, 2010, **132**, 13692.
28 A. J. Esswein, Y. Surendranath, S. Y. Reece and D. G. Nocera, *Energy Environ. Sci.*, 2011, **4**, 499.
29 J. B. Gerken, E. C. Landis, R. J. Hamers and S. S. Stahl, *ChemSusChem*, 2011, **3**, 1176.
30 J. B. Gerken, J. G. McAlpin, J. Y. C. Chen, M. L. Rigsby, W. H. Casey, R. D. Britt and S. S. Stahl, *J. Am. Chem. Soc.*, 2011, **133**, 14431.
31 Y. Liang, Y. Li, H. Wang, J. Zhou, J. Wang, T. Regier and H. Dai, *Nat. Mater.*, 2011, **10**, 780.
32 Y. Surendranath, D. A. Lutterman, Y. Liu and D. G. Nocera, *J. Am. Chem. Soc.*, 2012, **134**, 6326.

 This journal is © The Royal Society of Chemistry 2021

Open Access Article. Published on 05 August 2021. Downloaded on 9/22/2024 5:52:21 AM.
This article is licensed under a Creative Commons Attribution-NonCommercial 3.0 Unported Licence.

33 S. Cobo, J. Heidkamp, P.-A. Jacques, J. Fize, V. Fourmond, L. Guetaz, B. Jousselme, V. Ivanova, H. Dau, S. Palacin, M. Fontecave and V. Artero, *Nat. Mater.*, 2012, **11**, 802.
34 C. L. Farrow, D. K. Bediako, Y. Surendranath, D. G. Nocera and S. J. L. Billinge, *J. Am. Chem. Soc.*, 2013, **135**, 6403.
35 T. Y. Ma, S. Dai, M. Jaroniec and S. Z. Qiao, *J. Am. Chem. Soc.*, 2014, **136**, 13925.
36 Y. Liu and D. G. Nocera, *J. Phys. Chem. C*, 2014, **118**, 17060.
37 N. Jiang, B. You, M. Sheng and Y. Sun, *Angew. Chem., Int. Ed.*, 2015, **54**, 6251.
38 H. Kim, J. Park, I. Park, K. Jin, S. E. Jerng, S. H. Kim, K. T. Nam and K. Kang, *Nat. Commun.*, 2015, **6**, 8253.
39 Y. Zhao, S. Chen, B. Sun, D. Su, X. Huang, H. Liu, Y. Yan, K. Sun and G. Wang, *Sci. Rep.*, 2015, **5**, 7629.
40 G. Gardner, J. Al-Sharab, N. Danilovic, Y. B. Go, K. Ayers, M. Greenblatt and G. Charles Dismukes, *Energy Environ. Sci.*, 2016, **9**, 184.
41 H. Chen, Y. Gao and L. Sun, *ChemCatChem*, 2016, **8**, 2757.
42 L. Han, S. Dong and E. Wang, *Adv. Mater.*, 2016, **28**, 9266.
43 J. Wang, W. Cui, Q. Liu, Z. Xing, A. M. Asiri and X. Sun, *Adv. Mater.*, 2016, **28**, 215.
44 Y. Chen, J. Hu, H. Diao, W. Luo and Y.-F. Song, *Chem. Eur. J.*, 2017, **23**, 4010.
45 I. Roger, M. A. Shipman and M. D. Symes, *Nat. Rev. Chem.*, 2017, **1**, 0003.
46 S. E. S. El Wakkad and A. Hickling, *Trans. Faraday Soc.*, 1950, **46**, 820.
47 Y. Lattach, J. F. Rivera, T. Bamine, A. Deronzier and J.-C. Moutet, *ACS Appl. Mater. Interfaces*, 2014, **6**, 12852.
48 D. V. Morales, C. N. Astudillo, Y. Lattach, B. F. Urbano, E. Pereira, B. L. Rivas, J. Arnaud, J.-L. Putaux, S. Sirach, S. Cobo, J.-C. Moutet, M.-N. Collomb and J. Fortage, *Catal. Sci. Technol.*, 2018, **8**, 4030.
49 X. Cao, W. Yan, C. Jin, J. Tian, K. Ke and R. Yang, *Electrochim. Acta*, 2015, **180**, 788.
50 L. Liu, Y. Hou, J. Wang, J. Chen, H.-K. Liu, Y. Wu and J. Wang, *Adv. Mater. Interfaces*, 2016, **3**, 1600030.
51 Z. B. Shifrina, V. G. Matveeva and L. M. Bronstein, *Chem. Rev.*, 2020, **120**, 1350.
52 A. Zouaoui, O. Stephan, M. Carrier and J. C. Moutet, *J. Electroanal. Chem.*, 1999, **474**, 113.
53 A. Zouaoui, O. Stephan, A. Ourari and J. C. Moutet, *Electrochim. Acta*, 2000, **46**, 49.
54 Y. Lattach, A. Deronzier and J.-C. Moutet, *ACS Appl. Mater. Interfaces*, 2015, **7**, 15866.
55 D. W. Rice, P. B. P. Phipps and R. Tremoureux, *J. Electrochem. Soc.*, 1979, **126**, 1459.
56 B. H. R. Suryanto, X. Lu, H. M. Chan and C. Zhao, *RSC Adv.*, 2013, **3**, 20936.
57 C. Costentin, T. R. Porter and J.-M. Savéant, *J. Am. Chem. Soc.*, 2016, **138**, 5615.
58 C. N. Brodsky, D. K. Bediako, C. Shi, T. P. Keane, C. Costentin, S. J. L. Billinge and D. G. Nocera, *ACS Appl. Energy Mater.*, 2019, **2**, 3.
59 S. A. Bonke, M. Wiechen, R. K. Hocking, X.-Y. Fang, D. W. Lupton, D. R. MacFarlane and L. Spiccia, *ChemSusChem*, 2015, **8**, 1394.
60 A. S. Liu and M. A. S. Oliveira, *Mater. Res.*, 2007, **10**, 205.
61 S. P. Ozkorucuklu, Y. Sahin and G. Alsancak, *Sensors*, 2008, **8**, 8463.
62 T. W. Lewis, A Study of the Overoxidation of the Conducting Polymer Polypyrrole, Doctor of Philosophy thesis, Department of Chemistry, University of Wollongong, 1998, http://ro.uow.edu.au/theses/1107.
63 C. Costentin, T. R. Porter and J.-M. Savéant, *ACS Appl. Mater. Interfaces*, 2019, **11**, 28769.
64 S. Trasatti and O. A. Petrii, *Pure Appl. Chem.*, 1991, **63**, 711.
65 M. W. Louie and A. T. Bell, *J. Am. Chem. Soc.*, 2013, **135**, 12329.
66 C. C. L. McCrory, S. Jung, J. C. Peters and T. F. Jaramillo, *J. Am. Chem. Soc.*, 2013, **135**, 16977.
67 A. Singh, M. Fekete, T. Gengenbach, A. N. Simonov, R. K. Hocking, S. L. Y. Chang, M. Rothmann, S. Powar, D. C. Fu, Z. Hu, Q. Wu, Y. B. Cheng, U. Bach and L. Spiccia, *ChemSusChem*, 2015, **8**, 4266.
68 B. Klahr, S. Gimenez, F. Fabregat-Santiago, T. Hamann and J. Bisquert, *J. Am. Chem. Soc.*, 2012, **134**, 4294.
69 S. Anantharaj and S. Noda, *ChemElectroChem*, 2020, **7**, 2297.
70 R. L. Doyle and M. E. G. Lyons, *PhysChemChemPhys*, 2013, **15**, 5224.
71 M. E. Orazem, N. Pébère and B. Tribollet, *J. Electrochem. Soc.*, 2006, **153**, B129.
72 T. Pajkossy, *Solid State Ionics*, 2005, **176**, 1997.
73 A. J. Terezo, J. Bisquert, E. C. Pereira and G. Garcia-Belmonte, *J. Electroanal. Chem.*, 2001, **508**, 59.
74 I. M. F. De Oliveira, J. C. Moutet and S. Hamarthibault, *J. Mater. Chem.*, 1992, **2**, 167.
75 M. C. Biesinger, B. P. Payne, A. P. Grosvenor, L. W. M. Lau, A. R. Gerson and R. S. C. Smart, *Appl. Surf. Sci.*, 2011, **257**, 2717.
76 A. Foelske and H.-H. Strehblow, *Surf. Interface Anal.*, 2000, **29**, 548.
77 A. Han, H. Wu, Z. Sun, H. Jia and P. Du, *PhysChemChemPhys*, 2013, **15**, 12534.
78 H. Chen, Z. Sun, X. Liu, A. Han and P. Du, *J. Phys. Chem. C*, 2015, **119**, 8998.
79 Q. Daniel, R. B. Ambre, B. Zhang, B. Philippe, H. Chen, F. Li, K. Fan, S. Ahmadi, H. Rensmo and L. Sun, *ACS Catal.*, 2017, **7**, 1143.
80 C. Costentin and D. G. Nocera, *Proc. Natl. Acad. Sci.*, 2017, **114**, 13380.
81 D. K. Bediako, A. M. Ullman and D. G. Nocera, in *Solar Energy for Fuels*, ed. H. Tüysüz and C. K. Chan, Springer International Publishing, Cham, 2016, DOI: 10.1007/128_2015_649, p. 173.
82 N.-T. Suen, S.-F. Hung, Q. Quan, N. Zhang, Y.-J. Xu and H. M. Chen, *Chem. Soc. Rev.*, 2017, **46**, 337.
83 S. Anantharaj, S. R. Ede, K. Karthick, S. Sam Sankar, K. Sangeetha, P. E. Karthik and S. Kundu, *Energy Environ. Sci.*, 2018, **11**, 744.